

A generalized linear model of the impact of direct and indirect inputs to the lateral geniculate nucleus

Baktash Babadi¹, Alexander Casti^{2,4}, Youping Xiao², Ehud Kaplan², Liam Paninski^{1,3}

July 14, 2010

¹ Center for Theoretical Neuroscience, Columbia University, New York, NY, ² Department of Neuroscience, The Mount Sinai School of Medicine, New York, NY, ³ Department of Statistics, Columbia University, New York, NY, ⁴ Department of Mathematics, The Cooper Union School of Engineering, New York, NY

Abstract

Relay neurons in the Lateral Geniculate Nucleus (LGN) receive direct visual input predominantly from a single retinal ganglion cell (RGC), in addition to indirect input from other sources including interneurons, thalamic reticular nucleus (TRN) and the visual cortex. To address the extent of influence of these indirect sources on the response properties of the LGN neurons, we fit a Generalized Linear Model (GLM) to the spike responses of cat LGN neurons driven by spatially homogeneous spots that were rapidly modulated by a pseudo-random luminance sequence. Several spot sizes were used to probe the spatial extent of the indirect visual effects. Our extracellular recordings captured both the LGN spikes and the incoming RGC input (S potentials), allowing us to divide the inputs to the GLM into two categories: the direct RGC input, and the indirect input to which we have access through the luminance of the visual stimulus. For spots no larger than the receptive field center, the effect of the indirect input is negligible, while for larger spots its effect can on average account for 5% of the variance of the data, and for as much as 25% in some cells. The polarity of the indirect visual influence is opposite to that of the linear receptive field of the neurons. We conclude that the indirect source of response modulation of the LGN relay neurons arises from inhibitory sources, compatible with thalamic interneurons or TRN.

Key words: Lateral Geniculate Nucleus (LGN), S potentials, Generalized Linear Model (GLM), Retino-geniculate transmission

1 Introduction

As the prototypical sensory nucleus of the visual thalamus, the dorsal lateral geniculate nucleus (LGN) has been the subject of numerous studies for decades. However, the precise role of the LGN in processing visual information remains a matter of debate (Sherman and Guillery, 2002; Carandini et al., 2005; Sherman, 2005; Mante et al., 2008; Mayo, 2009; Rees, 2009). One reason for this is the complicated feedforward and feedback circuitry that drives and modulates relay cell responses (Sherman and Guillery, 1998), which makes isolation of the separate inputs difficult. Despite this, much progress has been made in demonstrating that non-retinal inputs to the relay cells significantly alter LGN activity, and enough is known to make a plausible case for the functional role of some of these effects (Andolina et al., 2007; Wang et al., 2007; McAlonan et al., 2008; Rees, 2009). To say that the LGN acts as more than a “mere relay” is now a cliché of neuroscience literature, replacing the older one to the contrary. The aim of this work is to probe the influence of non-retinal inputs with a quantitative statistical model, and to assess their importance in shaping fine details of LGN response.

Thalamic relay neurons receive strong feedforward excitation predominantly from one or two retinal ganglion cells (RGC) with overlapping receptive fields (Cleland et al., 1971; Usrey et al., 1999), from which the LGN neuron inherits the dominant features of its concentric, center-surround receptive field. A fundamental difference between the RGC and LGN receptive fields is a stronger, spatially extended inhibitory surround in the LGN, observed long ago by Hubel and Wiesel (1961). This enhanced inhibition likely originates in either local interneurons (Dubin and Cleland, 1977; Blitz and Regehr, 2005) or processes emanating from the thalamic reticular nucleus (TRN; Wang et al., 2001), with which the LGN is known to be reciprocally connected. The LGN and TRN also receive excitatory feedback from the cortex; together, the LGN, TRN, and cortex form a closed circuit in which each area has a reciprocal connection to the others. Thus, a key issue is the extent to which these extra-retinal sources influence the visual information processing of the LGN neurons.

Any model of the retinogeniculate pathway (Carandini et al., 2007; Casti et al., 2008) must account for the fact that the LGN transmits only a fraction of the retinal inputs it receives (see figure 1). It is clear from recordings that a single spike from the retina is sufficient (perhaps in conjunction with unseen inputs) to drive a relay cell past threshold, yet the fact is that in anesthetized preparations, on average, less than half of the primary driver ganglion cell inputs trigger an LGN spike (Kaplan et al., 1987). The LGN compensates for its lower firing rate by making each spike more informative (Sincich et al., 2009; Uglesich et al., 2009). This suggests that the mechanisms responsible for repressing LGN activity do so with a purpose and are not random.

The trend in recent studies of retinogeniculate (RG) transmission has been to find the simplest model or mechanism capable of explaining the variance in LGN relay cell recordings (Carandini et al., 2007; Casti et al., 2008; Sincich et al., 2009). Here, we take a different approach: we try to quantify the indirect visual influences on the RG transmission, no matter how modest, and examine its properties and physiological origin. By “indirect” visual influences we mean any visual input to the LGN relay cell beyond monosynaptic RG transmission. In our model we take advantage of single-cell extracellular recordings of LGN neurons that capture the timing of incoming retinal spikes in the form of S potentials (Bishop, 1953; Kaplan and Shapley, 1984). We thus have access to both the main input and the output of single neurons in the thalamus. Since the visual stimulus is under our experimental control, it is possible, by fitting a realistic neural model to these data, to examine whether the response of the LGN neuron to the visual stimulus is entirely governed by the direct monosynaptic retinogeniculate transmission, or whether some aspects of the LGN response are dictated by indirect sources of visual input. This is the underlying rationale of the method used in the present study. By fitting the parameters of a generalized linear model (GLM, Truccolo et al. 2005; Paninski et al. 2007) to the extracellular data, we show that the visual stimulus influences the response of the LGN neurons by paths other than the monosynaptic RG transmission. The time scales and spatial extent of the indirect contributions we found are consistent with feedforward inhibition from thalamic interneurons or feedback inhibition from the TRN.

2 Methods

2.1 Surgery

The experimental methods were similar to those described in Casti et al. (2008) in accordance with the National Institutes of Health guidelines and the Mount Sinai School of Medicine Institutional Animal Care and Use Committee. In brief, adult cats were anesthetized initially with an intra-muscular (IM) injection of xylazine (Rompun, 2 mg/kg) followed by ketamine hydrochloride (Ketaset, 10 mg/kg). Anesthesia was maintained with a mixture of propofol (4 mg/kg-hr) and sufentanil (0.05 μ g/kg-hr), which was given intravenously (IV) during the experiment. Propofol anesthesia has been shown to cause no changes in blood flow in the occipital cortex (Fiset et al., 1999), and appears to be optimal for brain studies. Phenylephrine hydrochloride (10%) and atropine sulfate (1%) were applied to the eyes. The animal was mounted in a stereotaxic apparatus. The corneas were protected with plastic gas-permeable contact lenses, and a 3 mm diameter artificial pupil was placed in front of each eye. Blood pressure, ECG, and body temperature were measured and kept within the physiological range. Paralysis was produced by an infusion of pancuronium bromide (0.25 mg/kg.h), and the animal was artificially respired. Such preparations are usually stable in our setup for more than 96 hours.

2.2 Visual Stimuli

Visual stimuli were presented monocularly on a CRT (mean luminance 25 cd/m²; frame rate 160 Hz) driven by a VSG 2/5 stimulator (Cambridge Research Systems, Cambridge, UK). Stimuli consisted of spatially homogeneous circular spots of various diameters, ranging from 0.5° to full field, modulated temporally according to a pseudo-random sequence (van Hateren, 1997; Reinagel and Reid, 2000). For each spot size we presented a sequence of 256 stimulus segments of random luminance modulation, each 8 seconds long, in which 128 repeated segments (repeats) were interleaved with 128 non-repeating segments (uniques). The entire stimulus run thus lasted $8 \times 256 = 2048$ seconds, during which the spot size was fixed. A filtered version of the repeated segment is shown in the top panel of figure 4A.

2.3 Recording of LGN spikes and S potentials

Extracellular recordings were taken from layers A and A1 of the LGN of 6 adult anesthetized adult cats. Amplified electrical signals were sampled at 40 kHz by a data acquisition interface (Spike 2, CED) for subsequent spike recording and sorting. To map the receptive field (RF) of LGN relay neurons, we first moved a mouse-controlled light or dark bar on the CRT to find

the approximate position of the RF, and then reverse correlated the spike train with a 16×16 checkerboard, in which each check (spanning 0.25° at 57 cm, in each linear dimension) was modulated by an independent m-sequence (Shutter, 1987; Reid et al., 1997). Neurons were classified as X or Y based on the responses to contrast reversal of fine gratings (Hochstein and Shapley, 1976). None of our Y cell recordings were sufficiently stable to be used in this work, so all the model results presented are for X cells. All cells were within 15° of the *area centralis*. The RF center size was estimated by fitting a Difference of Gaussians (DOG) model to the spatial response map that resulted from the reverse correlation procedure. The center radius was taken to be twice the standard deviation of the Gaussian fit. In the figures, spot sizes are reported as a multiple of the estimated size of the RF center, and are referred to as relative spot sizes.

When the electrode tip is sufficiently close to the LGN cell body, the retinal input to the relay cell can be captured in the form of slow synaptic potentials (S potentials), as shown in figure 1 (Bishop, 1953; Kaplan and Shapley, 1984). Because the electrode tip needs to be so close to the cell, we used finely tapered, high-resistance (10 M Ω) tungsten electrodes with platinum-black tip conditioning (FHC; epoxylite insulation). Despite the danger of damaging the cell in this type of recording, we were often able to hold the recordings for 12 hours or more with no apparent degradation in visual responsiveness. Owing to the length of each recording (> 4 hours) and the difficulty in obtaining S potentials that are easily discriminable over baseline noise, we typically were able to get just 1 or 2 successful recordings per animal that are suitable for the analysis presented here.

Spike times were determined off line by setting two threshold voltages: a low threshold of approximately 0.5 mV for the S potentials, and a higher threshold for the LGN spikes. An event time was defined by the threshold crossing at half height. As illustrated in figure 1, a single retinal S potential has variable success in eliciting an LGN relay cell response. A retinal input “failure” appears as an isolated, small-amplitude event, and a “success” manifests itself as a shoulder on the rising phase of the large-amplitude relay cell spike it triggers. The S potential is fused with the relay cell spike to various degrees, sometimes separated entirely from the action potential by ~ 1 ms (Sincich et al., 2007; Weyand, 2007). In cases where a retinal input induced an LGN spike, our method of detecting S potentials created a slight delay between the S potential and the LGN spike time, ranging from 0 to 1 ms, depending on the extent to which the S potential was embedded within the LGN spike. For a small fraction ($< 5\%$) of LGN events, the presence of a spike-triggering S potential is not detectable in the extracellular trace either within the spike or nearby. In these cases it is possible that the most recent S potential served to “prime” the relay cell, allowing another, perhaps smaller, input to drive it past threshold. Whatever the case, whether an S potential is detectable or not, we assume in the model that each LGN spike has an S potential accompanying it. The validity of this assumption has received experimental support in recordings from both anesthetized (Sincich et al., 2007) and awake (Weyand, 2007) preparations. In all the cells analyzed, successive S potentials arrived at intervals > 2 ms, making it unlikely that there were two or more dominant drivers from separate ganglion cells.

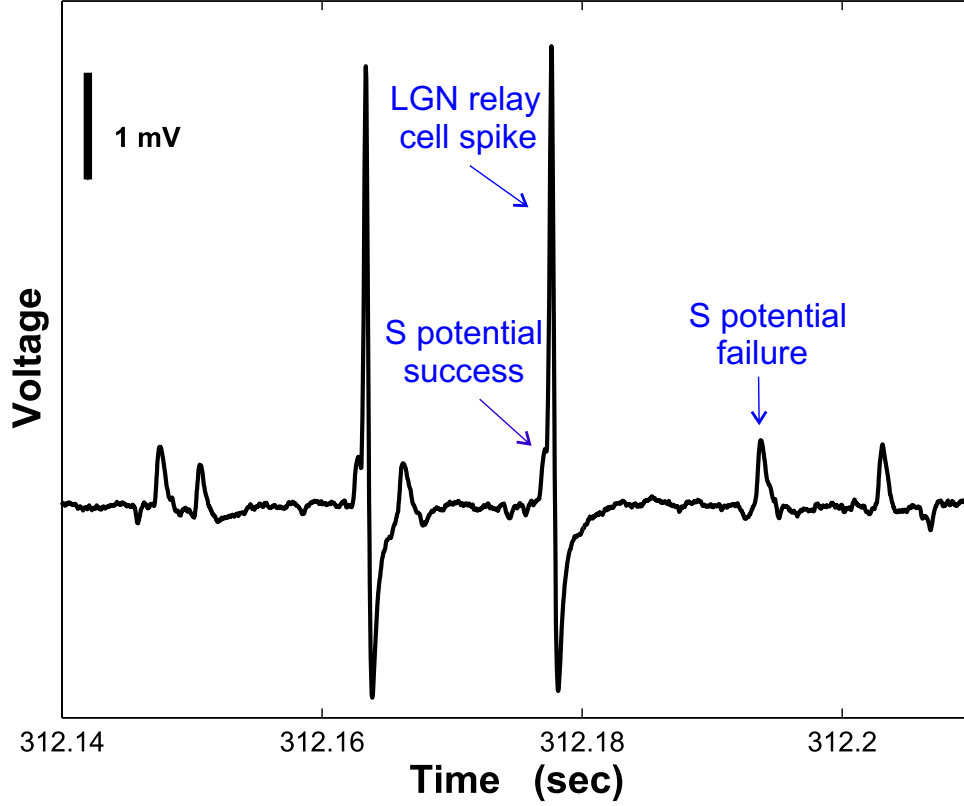


Figure 1: An example extracellular voltage recording of an LGN neuron, corresponding to the cell in figure 5B. This record shows seven S potentials, which are large EPSPs driven by RGC input spikes. A “failed” S potential does not have a concomitant LGN spike, while a “successful” S potential is typically embedded within an LGN spike.

2.4 Modeling and data analysis

To estimate distinct contributions to the response of LGN neurons, we fit a Generalized Linear Model (GLM, Paninski 2004; Paninski et al. 2007) to the stimulus and spike train data. The GLM in this case has the form

$$\lambda_t = f \left(b + \sum_{i=1}^{\dim D} D_i x_{t-i+1} + \sum_{j=1}^{\dim H} H_j n_{t-j} + \sum_{m=1}^{\dim K} K_m l_{t-m+1} \right). \quad (1)$$

The inputs to the model are x_t , n_t and l_t , which represent discrete time series for the RGC spikes (S potentials), LGN spikes, and the luminance of the visual stimulus at time t , respectively. A distinct linear temporal filter is convolved with each source of input to the model: The filter \vec{D} acts on the RGC spikes (x_t), the filter \vec{H} acts on the past LGN spikes (n_t) and models the spike-history effects on the present activity of the neuron, and the filter \vec{K} acts on the luminance of the visual stimulus (l_t). The parameter b is a constant offset that defines the background firing rate of the LGN neuron. Because of the presence of the constant b , which represents the sum of all constant inputs to the function f , the filters are mainly responsive to deviations of the corresponding inputs around their means. In line with this inherent separation of mean and variance in the model and in order to make the interpretation of the filter \vec{K} more clear, we subtracted the mean luminance (25 cd/m²) from the values l_t at each time. After convolving the inputs with the filters, the result is fed into a nonlinear, monotonically increasing function f to calculate the instantaneous firing rate λ_t of the LGN neuron at time t . The main role of f is to capture nonlinear thresholding effects. Finally, the number of spikes in each time bin of duration dt is drawn from a Poisson distribution such that $n_t \sim \text{Pois}(\lambda_t dt)$. Figure 2 depicts a schematic structure of the GLM and its components. An important feature of the GLM used here is that the visual input enters through two distinct routes: first, from the RGC spikes (x_t) with its corresponding temporal filter \vec{D} , and second, through the luminance of the visual stimuli (l_t), with its corresponding filter \vec{K} (which we call the “luminance” or “indirect” filter). The rationale for incorporating the latter in the model is to account for possible information about the visual stimulus that affects the response of the LGN neuron, but is not directly mediated by

the RGC spike train to the LGN neuron. Thus, the filter \vec{D} represents the monosynaptic RG transmission, whereas \vec{K} filters stimulus information beyond that directly transmitted to the LGN by the retina (such as cortical feedback and intrageniculate inhibition).

In order to simplify the notation, the inputs to the model can be lumped into a single vector as

$$\vec{X}_t = [1 \quad x_t \dots x_{t-\dim(D)+1} \quad n_{t-1} \dots n_{t-\dim(H)} \quad l_t \dots l_{t-\dim(K)+1}] .$$

The parameters of the model, i.e. the constant offset and the linear temporal filters, can also be lumped into the single vector

$$\vec{\theta} = [b \quad \vec{D} \quad \vec{H} \quad \vec{K}] .$$

Now equation (1) can be re-written as

$$\lambda_t = f(\vec{\theta} \cdot \vec{X}_t) . \quad (2)$$

The log-likelihood L of the GLM producing the observed LGN spike train (O) can be written as in Snyder and Miller (1991):

$$L = \log p(O | \vec{X}, \vec{\theta}) = c + \sum_t \left(n_t \log f(\vec{\theta} \cdot \vec{X}_t) - f(\vec{\theta} \cdot \vec{X}_t) \right) dt , \quad (3)$$

where c is a constant unrelated to the model parameters. If $f(u)$ is a convex function of its scalar argument u , and $\log f(u)$ is concave in u , then the above log-likelihood is guaranteed to be a concave function of the parameter $\vec{\theta}$, since in this case the log-likelihood is just a sum of concave functions of $\vec{\theta}$ (Paninski, 2004). This ensures that the likelihood has a unique maximum for some parameter vector $\vec{\theta}_{ML}$, which can be found easily by numerical ascent techniques. We use the standard Hessian-based estimate for the standard error of the optimization: $\text{diag} \left[(\nabla_{\vec{\theta}_{ML}}^2 L)^{-1} \right]^{\frac{1}{2}}$ provides error bars for each corresponding entry in the parameter vector $\vec{\theta}$, where $\nabla_{\vec{\theta}_{ML}}^2 L$ denotes the Hessian of the log-likelihood evaluated at the maximum likelihood estimate $\vec{\theta}_{ML}$ (Paninski (2004); Truccolo et al. (2005); Paninski et al. (2007); see figures 3 and 5). The function $f(u)$ used here that satisfies the above conditions is:

$$f(u) = \log(1 + e^u) . \quad (4)$$

Other choices of convex and log-concave functions (including exponential and quadratic) did not alter the results of this study.

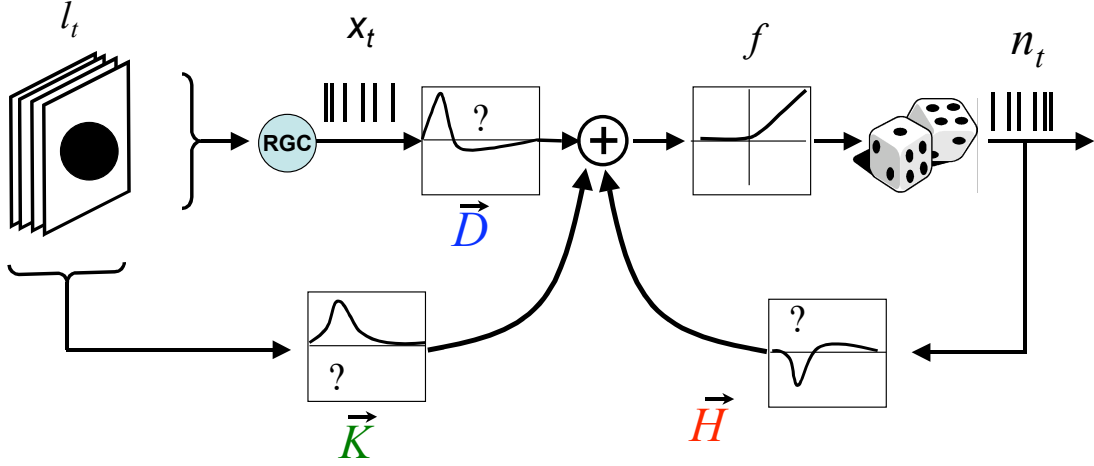


Figure 2: A schematic of the GLM that is fit to the recorded LGN data. The inputs to the model are the RGC input events x_t (S potential times; figure 1), the LGN cell spike time history n_t , and the luminance of the visual stimulus l_t . The linear filters acting on the inputs are \vec{D} (blue), \vec{H} (red) and \vec{K} (green). A static nonlinearity f (equation 4) transforms the sum of filtered inputs to obtain the instantaneous firing rate of the neuron. The output spikes are generated as an inhomogeneous Poisson process with the rate parameter λ_t given by equation (1). The model inputs derive from the experimental data, while the linear filters are given by maximizing the likelihood of the model that reproduces the experimental LGN spike train. The temporal filter \vec{D} represents the monosynaptic retinogeniculate transmission, and the filter \vec{K} captures the effects of indirect visual inputs.

For each stimulus size the recorded data consist of LGN responses to 128 unique and 128 repeated trials. The parameters of the model ($\vec{\theta}$) are optimized by maximizing the log-likelihood (equation 3) of the model in reproducing the spike train of the unique trials. Thereafter, the repeated trials (which are not part of the GLM training data) are used to cross-validate the model. To assess the quality of the model fit to the observed data, we calculated the percentage of the variance in the post-stimulus time histogram (PSTH) of the recorded LGN data accounted for by the GLM for the repeated trials (Pillow et al., 2005):

$$r = 100 \times \left(1 - \frac{\langle (\text{PSTH}_{\text{data}} - \text{PSTH}_{\text{model}})^2 \rangle}{\langle (\text{PSTH}_{\text{data}} - \langle \text{PSTH}_{\text{data}} \rangle)^2 \rangle} \right), \quad (5)$$

where $\text{PSTH}_{\text{data}}$ and $\text{PSTH}_{\text{model}}$ refer to the PSTH of the laboratory data and the GLM, respectively, and $\langle \cdot \rangle$ denotes a time average across trials. We computed the PSTH using a bin width of 6.25 ms, equivalent to the frame interval of the 160 Hz stimulus presentation on the CRT. For each experimental condition, two GLMs are fit to the observed LGN spike trains. First, a full model that contains all the temporal filters (\vec{D} , \vec{H} and \vec{K}); and second, a GLM that lacks the indirect filter \vec{K} . Comparison of these two models provides the contribution of the indirect or extra-retinal routes of visual input to the LGN response.

Note that the time courses of the three filters \vec{D} , \vec{H} , and \vec{K} indicate LGN spike probability contributions of different events that happen at different times. Relative to the “zero time” (the time at which the filters are convolved with the input and spike histories), a peak in the retinal filter \vec{D} roughly corresponds to the most recent post-synaptic S potential event at the LGN cell body. A trough in the \vec{H} filter is associated with the suppression that generally follows the most recent LGN action potential, and a peak or trough in the indirect kernel \vec{K} is associated with the stimulus history as it appeared on the laboratory monitor. To get an estimate of the relative time delay between relay cell responses and any indirect inputs, we compare the time evolution of the \vec{K} filter with the time evolution of the LGN linear receptive field at the RF center, as given by reverse correlation with a spatio-temporal m-sequence (see section 2.3).

3 Results

We optimized the parameters of the GLM for 10 recorded LGN neurons (6 X-Off and 4 X-On cells). Figure 3 shows the optimized temporal filters for two representative LGN neurons. Before discussing the contributions of each model component to the LGN response, we evaluate the overall performance of the model in capturing the statistical properties of the recorded LGN spike trains.

3.1 Statistics of the LGN discharge

Figure 4A juxtaposes the response of a recorded X-Off LGN neuron and the GLM fit to the repeated trials. As can be seen, the full GLM can accurately reproduce the instantaneous firing rate and the variance of the firing rate of the real neuron across different trials. The inter-spike-interval (ISI) distribution of the spikes generated by the GLM also matches that of the real neuron (figure 4B); similar results were observed for the other analyzed cells (data not shown).

Apart from the statistical parameters of the LGN response, the GLM can capture other important features of LGN response as well. For instance, in both the real data and the model, the LGN neuron produces fewer spikes than the RGC neuron. Thus each S potential is not necessarily accompanied by an LGN spike (figure 4A, rasters). Some S potentials succeed in being transmitted by LGN to the visual cortex and some fail (Carandini et al., 2007; Casti et al., 2008; Uglesich et al., 2009); in this data set, the “transfer ratio” (the number of LGN spikes divided by the number of retinal S potentials) was 0.24 (i.e., about one quarter of S-potentials triggered an LGN spike). The GLM predicted a similar transfer ratio ~ 0.24 . Both in the real data and in the model, the failed S potentials tend to cluster prior to successful S potentials accompanied by an LGN spike (Figure 4A, ovals); this phenomenon is well-explained by temporal summation of RGC inputs, as has been shown previously (Carandini et al., 2007; Casti et al., 2008); see the Discussion section.

3.2 The GLM filters

For all spot sizes and for both RF center polarities (On and Off), the time course of the estimated RGC filter \vec{D} is approximately an exponential decay with a time constant of ~ 20 ms (figure 3, blue curves). The spike history filter \vec{H} is also approximately exponential, but is negative (suppressive), and has a shorter time constant (~ 5 ms) for all spot sizes (figure 3, red curves). The filters \vec{D} and \vec{H} were traced back up to 30 ms prior to the stimulus time t . For times longer than that, these filters were effectively zero, and taking them into account only slowed down the optimization process. Moreover, using the repeated trials to cross-validate the model with filters having more time bins showed that adding redundant time bins to the model filters did not improve the fit, and eventually made the fit worse. This can be due to over-fitting of the model to the details of the noise in the data. . With these considerations in mind, we found a 30 ms history to be appropriate for the GLM optimization.

The luminance filter \vec{K} is most significant in time intervals beyond the range of the \vec{D} and \vec{H} filters: It has a peak around 40 – 45 ms after stimulus onset for the Off cells (figure 3A) and a trough around the same time for the On cells (figure 3B). To give this result some physiological context, we compared the time evolution of \vec{K} with the first order temporal linear kernel (i.e. the temporal receptive field; figure 3 insets). The linear receptive field has a peak for the On cells and a trough for the Off cells, both appearing about 35 ms after stimulus onset. Thus, the \vec{K} filter is about 5 – 10 ms delayed compared to the peak response of the LGN neurons. The \vec{K} filter represents the combined effect of the visual response of a presynaptic neuron plus the synaptic transmission to the LGN cell. Therefore, any positive or negative fluctuations in \vec{K} can have a variety of interpretations. A positive excursion (a peak) in the \vec{K} filter can be due to an excitatory input with an On origin, or an inhibitory input with an Off origin. Similarly, a negative excursion (a trough) in the \vec{K} filter can be attributed to an excitatory Off or an inhibitory On input. Alternatively, since the \vec{K} filter is tuned to variations of the luminance around its mean, a peak can be interpreted as the removal of an excitatory Off or inhibitory On input. Finally, a trough can be interpreted as the removal of an excitatory On or inhibitory Off input. Although a linear model (up to spike generation) like ours cannot in principle distinguish between increased inhibition and decreased excitation, in what follows we will discuss all the above possibilities in light of the available literature about thalamic circuitry, and argue that the indirect visual influence corresponds to an inhibitory source, possibly with an opposite polarity to the RF center of the LGN relay cell (see discussion).

While the RGC and spike history filters do not vary with the size of the visual stimulus, the luminance filter \vec{K} changes as a function of spot size. Figure 5 shows the progression of the \vec{K} filter for different visual spot sizes, corresponding to the representative Off and On cells in figure 3. The magnitude of the luminance filter \vec{K} is almost zero for small spot sizes, and becomes more significant as spot size increases. The magnitude of the \vec{K} filter tends to shrink again for even larger spot sizes. Among other things, this suggests the absence of indirect excitation or inhibition for small spot sizes, and enhanced inhibition

at larger spot sizes. If this indirect effect were due to decreased excitation, then we would have expected to see evidence of indirect excitation at small spot sizes. It is worth noting that in some cells the \vec{K} filter may show a polarity reversal for later times (e.g. 3B). This is expected as the luminance filter itself indirectly originates from the activity of a RGC whose temporal RF is typically biphasic.

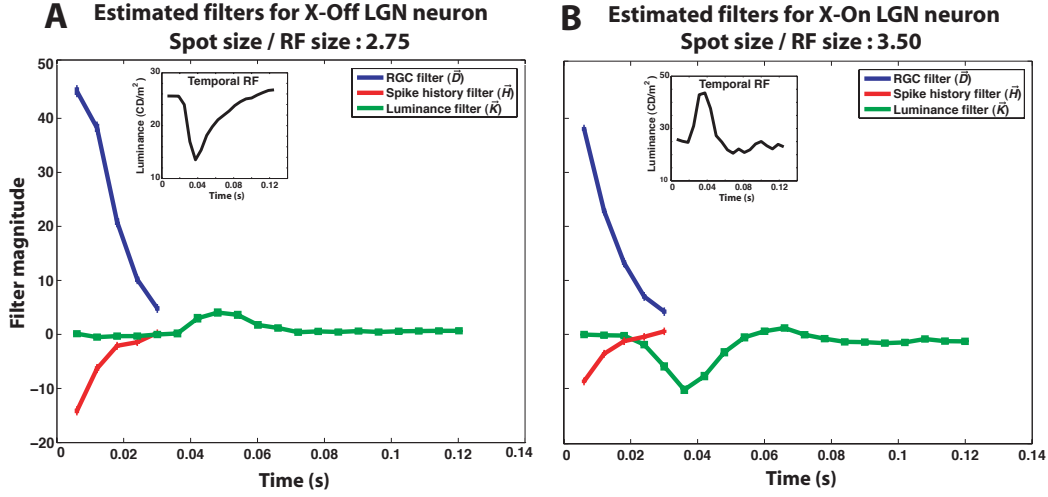


Figure 3: An example of the optimized linear temporal filters for A)an X-Off LGN neuron and B)an X-On LGN neuron. The error bars indicate the standard error of the optimization for each point (see Methods). The time course of the response of each cell, obtained by reverse correlation with checkerboard m-sequence stimuli (section 2.3), is shown in the insets. Each filter is normalized by the standard deviation of its corresponding input, so that the magnitude of the three filters may be compared directly.

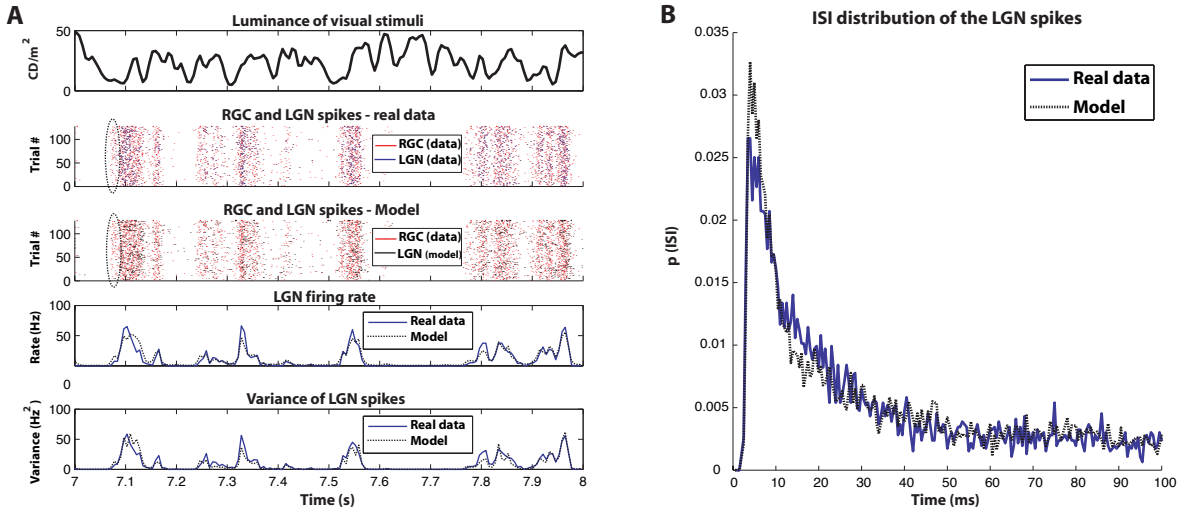


Figure 4: The spike train of the GLM compared to the recorded (real) spike train of the LGN X-Off neuron from figure 3A, for the 128 repeated trials. **A)** The luminance of the visual stimulus is shown in the top panel; the RGC spikes (red) and the real LGN spikes (blue) are shown in the second panel. In the third panel the same RGC spikes (red) and the spike trains of the model LGN neuron (black) are illustrated. The ovals highlight the tendency of the RGC spikes to cluster before the LGN spikes both in the real data and the model. The fourth panel shows the instantaneous firing rate of the real (blue) and model (dotted black) LGN neurons averaged across trials. The bottom panel shows the variance of the firing rate for real (blue) and model (dotted black) LGN neuron across trials. **B)** The inter-spike-interval (ISI) distribution of the spike trains of the real (blue) and model (dotted black) LGN neurons.

3.3 Contribution of direct visual input

To quantify the indirect contribution of luminance information through the \vec{K} filter on the RG transmission – as opposed to the contribution from the RGC input and its associated \vec{D} filter – we fit a GLM without the \vec{K} filter to have a baseline for comparison. We then calculated the performance of the full model and the model without the \vec{K} filter according to equation (5). Figure 6A shows the performance of the GLMs for a representative Off cell, and figure 6B illustrates the same results for a representative On cell (corresponding to figures 3 and 5, respectively). Incorporating the luminance filter \vec{K} into the model generally improves the fit, particularly for mid-range stimulus sizes. This finding is more evident in figures 6C and 6D, where the contribution of \vec{K} filter is demonstrated as a function of the stimulus size. For the mid-ranged spot sizes the \vec{K} filter increases the performance of the GLM up to 7% for both cells.

The bar charts in figure 7 show the average performance of the GLMs with and without the luminance filter \vec{K} , together with the contribution of \vec{K} for three ranges of the relative stimulus size for all the recorded cells. In general, the model performs better for smaller spots and the contribution of \vec{K} filter increases for larger spots. Figure 8 shows the contribution of the luminance filter \vec{K} as a function of the stimulus size for all 10 recorded LGN neurons. Here also a clear trend is visible: the \vec{K} filter contributes to the LGN response predominantly for stimuli that are larger than the receptive field center. The maximum contribution of the \vec{K} filter can reach up to 25% for some cells, though in most cases the contribution is smaller. The data from some of the cells analyzed here were also used in previous studies from our group (Casti et al., 2008; Uglesich et al., 2009), as indicated in the inset of figure 8.

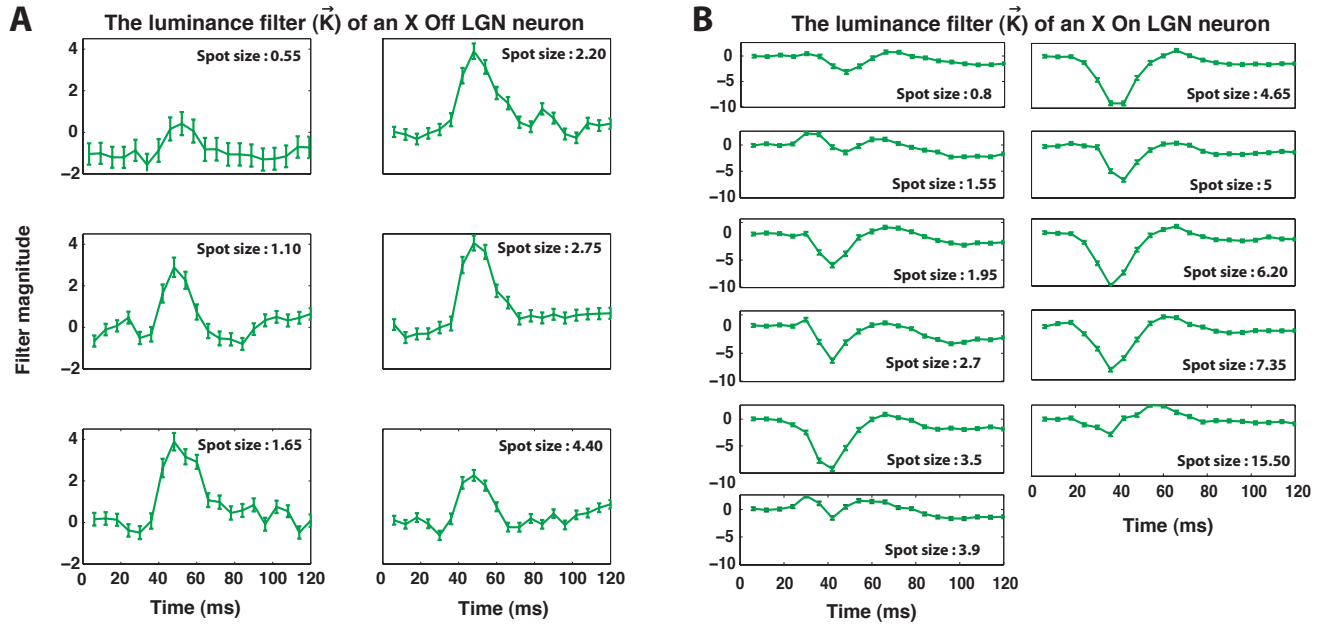


Figure 5: The luminance filter \vec{K} for several spot sizes (relative to the RF center size), **A)** for the representative Off cell corresponding to figure 3A and **B)** for a representative On cell corresponding to figure 3B. The error bars show the standard error of the optimization for each point (see Methods).

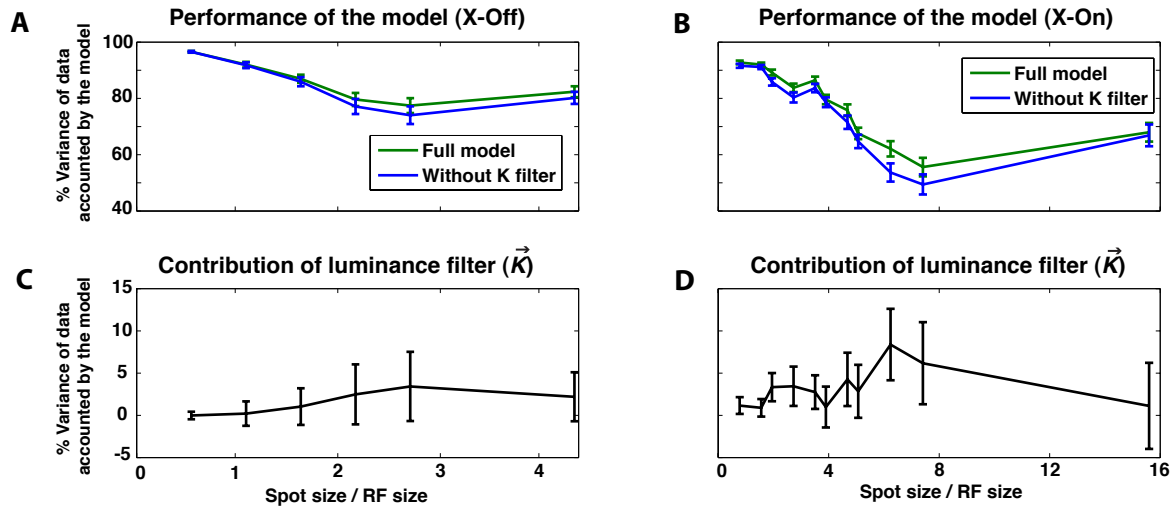


Figure 6: The performance of the GLMs and the contribution of the luminance filter (\vec{K}). **A)** The performance of the GLM in reproducing the real LGN spike trains in the repeated trials, calculated according to equation 5. The graph shows the performance of the full GLM (green) and the GLM without \vec{K} filter (blue) as a function of the relative size of the stimulus spot, for the same Off cell as in figures 3A and 5A. **B)** Similar results for the representative On cell of figures 3B and 5B. **C)** The contribution of the luminance filter \vec{K} in improving the performance of the GLM for the representative Off cell. **D)** The same results for the representative On cell. Error bars indicate the standard deviation over the 128 repeated trials in each case. Note that the contribution of the **luminance** filter is fairly small.

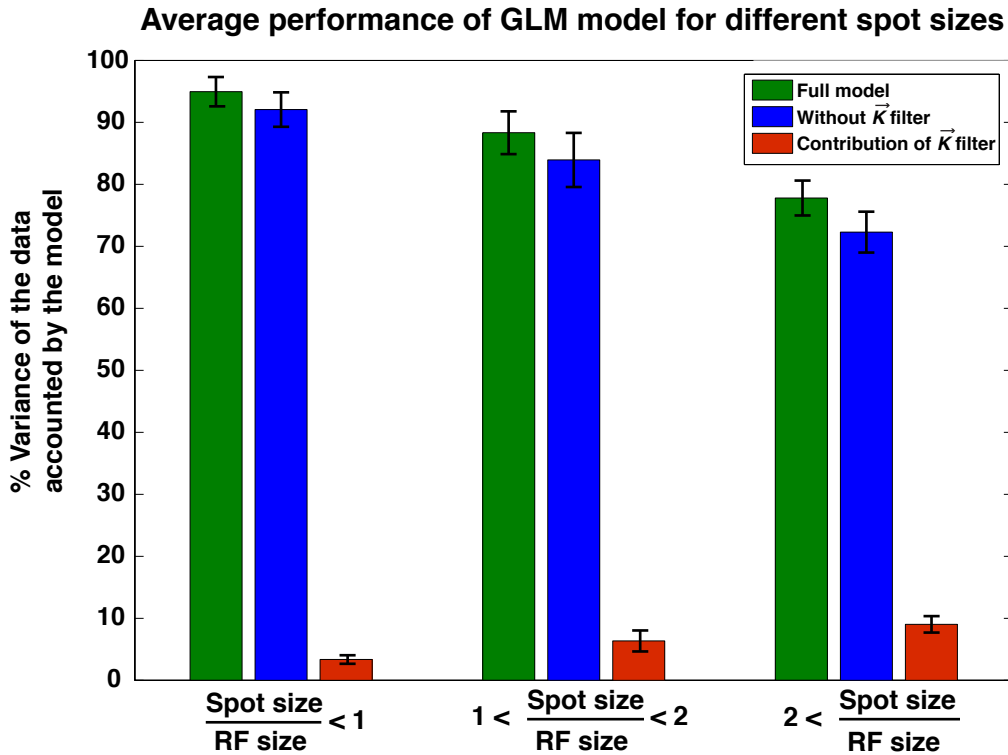


Figure 7: The average performance of the GLMs and the contribution of the luminance filter (\vec{K}) for different relative spot sizes. The performance of the model is calculated according to equation (5). The GLM predicts the LGN response better for small stimuli. The contribution of the luminance filter (\vec{K}) increases for larger stimuli. The error bars depict the standard error.

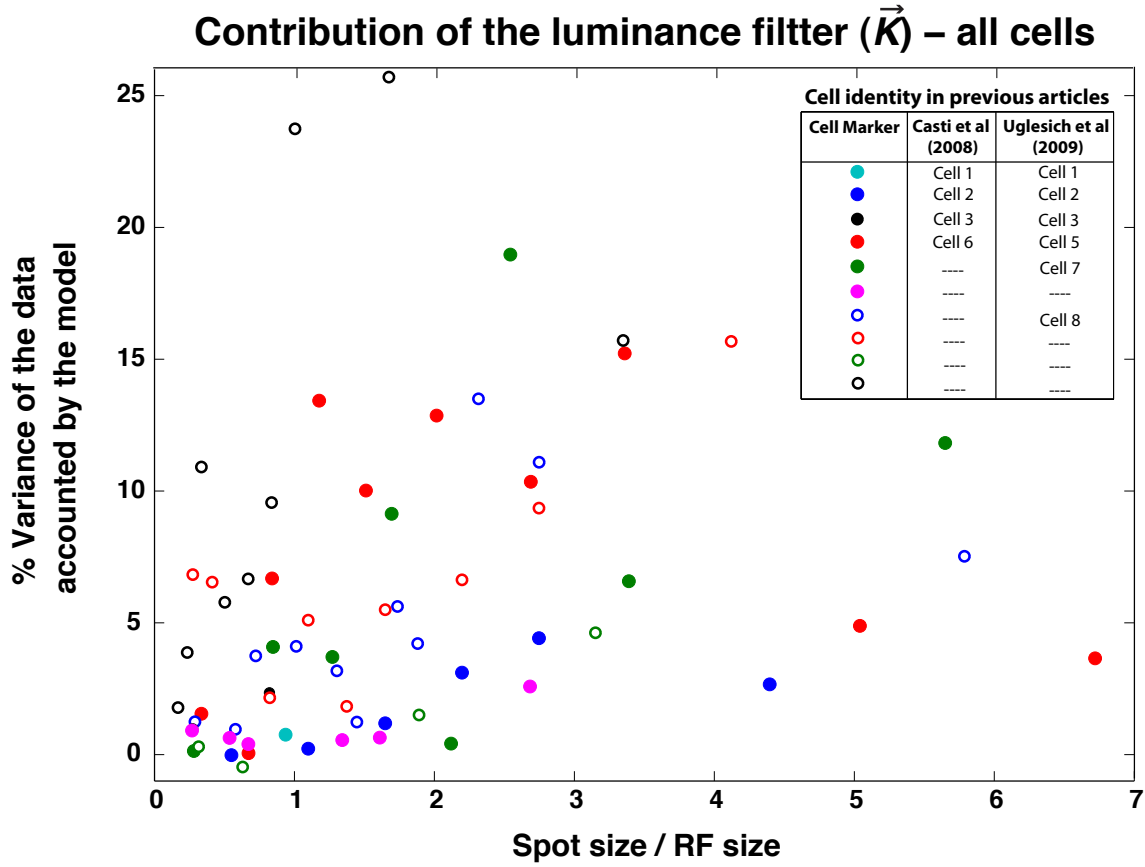


Figure 8: The contribution of the luminance filter \vec{K} to the performance of the GLM for all 10 analyzed LGN neurons. The horizontal axis indicates the relative spot size. The vertical axis indicates the contribution of the \vec{K} filter (in the percentage units illustrated in figure 6). Each marker shows the results for a single neuron and a specific stimulus size. The filled circles represent Off cells and open circles represent On cells. Each color corresponds to a distinct cell. The inset shows the identity of the cells that were also analyzed in two previous articles of our group.

4 Discussion

In order to quantify the effect of indirect visual inputs to the LGN relay neurons, we fit a generalized linear model to spike trains recorded from these neurons, along with their RGC inputs (as reflected by the recorded S potentials), while the size of the visual stimulus was varied systematically. We found that the indirect input sources are most significant for stimulus sizes that were more than two times larger than the diameter of the RF center of LGN neurons.

The GLM class of models is a natural mathematical extension of the basic physiological concept of a “receptive field” that also includes spike-history effects such as refractoriness, burstiness and adaptation. Because of the separation of linear and nonlinear components and the incorporation of spike-history effects into the linear component, the GLM is well suited for modeling neural spike trains, and gives an intuitive explanation of the underlying neuronal processes. In fact, the GLM has proved useful in a wide variety of experimental preparations (Pillow et al., 2005; Truccolo et al., 2005; Okatan et al., 2005; Pillow et al., 2008), and has been shown in many cases to be of comparable accuracy to the more widely used integrate-and-fire (IF) model (Paninski et al., 2007). In the particular case of LGN response, IF model neurons with a biologically realistic circuitry have been used to predict experimental data similar to those of the present study (Casti et al., 2008). The accuracy of the GLM is quite comparable to that of the IF model in this case (i.e. more than 90% variance captured for small spots and around 80% for large spot stimuli). The IF model has the advantage of matching more closely the physiological intuition about the neural circuits, at the expense of losing the speed and guarantee of finding the optimal parameters, which are inherent in the GLM. The GLM retains most of the appealing biophysical interpretations of the individual model components of the IF type models, and very often offers significant computational savings in the optimization. Besides the general properties of the GLM, what made this model an appropriate choice in the present study was the availability of the retinal S

potentials, which allowed us to separate in the model the direct retinal input from the other, less easily detected inputs. In the present study, we detected a statistically significant, though modest, contribution of inhibitory inputs to the performance of a generalized linear model. That we were able to capture these effects highlights an important distinction between GLM and IF models: while the performance of the IF model is restricted by the specifics of the implemented circuitry (such as fixed synaptic delay, polarity of the inhibitory input, etc), the components of the GLM are more phenomenological, and do not require an *a priori* implementation of the specific biophysical properties. It is, therefore, more flexible in revealing the factors influencing the neural response.

Both the exponentially decaying shape and the time course of the estimated RGC filter \vec{D} here are consistent with retinogeniculate synaptic transmission. The results show that on average the RGC input component of the model accounts for more than 90% of the variance of the observed LGN activity in all stimulus conditions. Although the contribution of indirect inputs in the LGN visual response may reach up to 25% for some neurons, it is generally small compared to the monosynaptic retinogeniculate transmission. This result is in line with previous studies showing that the LGN response is predominantly governed by the RGC driving input and the post-synaptic temporal summation of S potentials (Cudeiro and Sillito, 1996; Sincich et al., 2007; Carandini et al., 2007; Casti et al., 2008). In particular, although the S potentials that fail to elicit an LGN spike depolarize the membrane potential of the LGN neuron, they are not sufficient to push it over the spiking threshold. However, these “failures” make it easier for subsequent S potentials to evoke an LGN spike. Therefore, the tendency of the RGC spikes to cluster before the LGN spikes, as shown in figure 4, could be explained solely by temporal summation of RGC inputs (Carandini et al., 2007; Casti et al., 2008). The same short-term temporal summation has been shown (Sincich et al., 2009; Uglesich et al., 2009) to account for the majority of the formal information (bits) transmitted by LGN relay neurons. These recent studies have shown that LGN relay neurons re-encoded features of the visual stimulus so that each output spike carried more information about the stimulus than each RGC spike. Further, Sincich et al. (2009) found that the most informative dimension in the vector space of RGC inputs corresponds to a monotonically increasing function that starts to deviate from zero around 35 ms before the LGN spike. This analysis is compatible with the temporal summation of RGC spikes within a 35 ms window before the LGN spike.

In our GLM, all potential indirect inputs are lumped into the single luminance filter \vec{K} . Although the contribution of the indirect inputs in shaping the LGN response is modest compared to the direct retinogeniculate transmission, our results enable us to put forward a few conjectures about its origin. As mentioned before, the GLM *per se* cannot distinguish between excitatory or inhibitory origin of the \vec{K} filter. Although there is evidence that LGN relay neurons may receive weak excitatory input from a few RGC cells other than their main excitatory drive (Cleland et al., 1971; Hamos et al., 1987; Usrey et al., 1999; Wang et al., 2007), the receptive fields of those RGCs are tightly overlapping and have the same polarity as the main RGC/LGN neuron (Usrey et al., 1999). The luminance filter \vec{K} has an excitatory effect on Off cells and an inhibitory effect on On cells, which was observed in all 10 neurons we analyzed. Its polarity is therefore opposite to that of the temporal linear receptive field of the LGN neuron. An excitatory origin with the same polarity as the LGN neuron cannot explain the reversal of the polarity of the observed \vec{K} filter. The maximum effect of the \vec{K} filter has a $\sim 40 - 45$ ms delay with respect to the stimulus onset (figure 3), while the peak response of the linear temporal receptive fields of LGN neurons occurs about ~ 35 ms after the stimulus onset, giving an approximate relative delay of $\sim 5 - 10$ ms between the retinal excitation at the LGN cell body and the indirect input. Again, the $5 - 10$ ms delay of the peak (or the trough in case of On cells) of the \vec{K} filter is not compatible with a feed-forward excitatory input from other RGCs. When all spot sizes are considered, our results are consistent with the interpretation of these indirect effects as inhibition, as we found no evidence for indirect excitation at small spot sizes ($\sim 0.5 - 1$ times the RF center size). The greater impact of the contribution of the \vec{K} filter for larger stimuli implies that the receptive field of the inhibitory source is either larger than the receptive field of the LGN neuron itself, or displaced towards its receptive field periphery.

4.1 Sources for inhibition

The above mentioned properties of the observed indirect visual input seem consistent with a local feed-forward interneuronal source or feedback inhibition from the TRN (or both). Interneuronal inhibition was found to be prominent in the intracellular recordings from LGN relay neurons by Wang et al. (2007), who had access to both the excitatory (EPSCs) and inhibitory (IPSCs) inputs to visually driven relay neurons. They mapped the RF of both inhibitory and excitatory inputs and showed that the inhibitory input most likely arises from thalamic interneurons with an overlapping center-surround receptive field structure similar to the LGN relay neurons (Dubin and Cleland, 1977; Humphrey and Weller, 1988; Sherman and Friedlander, 1988). It has been shown that the polarity of the receptive field of the inhibitory input is opposite to that of the LGN target, resulting in a pull inhibitory effect (Wang et al., 2007). Our results deviate from this strict pull inhibitory input. For instance,

in the case of pull inhibition to an Off LGN neuron, the inhibitory interneuron responds to On transitions in the stimulus (dark to bright). Therefore, such an interneuron would inhibit the LGN cell for bright spot stimuli, and the \vec{K} filter would have to be negative even for small spot stimuli. However, we observed no significant \vec{K} filter influence for small spots, and for larger spots it is positive, contrary to what one would expect of pull inhibition. One possible explanation is that the \vec{K} filter represents a partial removal of a pull inhibitory input for larger spots that hit the surround of the RF of the inhibitory interneuron. Neurons in the TRN, on the other hand, have large receptive fields that are often less well-organized compared to LGN relay neurons (Uhlrich et al., 1991). The TRN activity is also a plausible source for the inhibition we observe since it tends to be anti-correlated with LGN responses. This has been observed for retinotopically matched LGN and TRN cells in anesthetized cat (Funke and Eysel, 1998) and awake monkey (McAlonan et al., 2008) preparations. The 5 – 10 ms delay between the observed inhibition and the relay cell peak response could accommodate a round trip to V1 and back to the LGN through the TRN (Briggs and Usrey, 2007).

The feedforward inhibitory input arising from intra-thalamic interneurons is classified into two distinct types with presumably different physiological roles (Blitz and Regehr, 2005). The “locked” feedforward inhibition, which is observed in $\sim 33\%$ of relay cells, is tightly correlated with the excitatory input, and is believed to arise from the same RGC as the excitatory input. In contrast, the “nonlocked” feedforward inhibition seen in $\sim 67\%$ of relay cells is believed to originate from RGCs other than the main excitatory drive of the LGN cells. The locked variety of inhibition has been suggested as a mechanism for sharpening the precision of LGN responses, while the unlocked type provides surround inhibition to LGN receptive fields (Blitz and Regehr, 2005). Since the maximum effect of the inhibitory input in our data is observed when the size of the spot stimulus is larger than the receptive field center, this suggests that the indirect visual influence we observe tallies better with the nonlocked feedforward inhibition that arises from RGC neurons in the vicinity of the predominant excitatory driver of the LGN neuron. This does not imply the complete absence of a form of locked inhibition driven by the primary RGC input, but in the context of our GLM and stimulus paradigm it means that such influences contribute little to the model performance, or cannot be disambiguated from the spike history filter \vec{H} . If pull inhibition played a prominent role in the generation of LGN burst events, as implied by the results of Wang et al. (2007), who used natural stimuli, then perhaps this form of inhibition would have been captured in our model if we had used a different stimulus. Further, a time scale of 5 – 10 ms before the onset of the inhibition seems too long to implicate a locked form of inhibition, and would be more consistent with disynaptic inhibition originating in other ganglion cells that might be spread across multiple interneurons with variable delays. Richer stimuli may reveal further details about the shape, location, and origin of the indirect visual inputs to the LGN relay neurons. Also note that we did not include Y cells in the present study as they did not yield stable recordings of S potentials. Whether the indirect inputs play a similar role in those cells is an open question.

Due to the limitations of extracellular recording and the phenomenological nature of the GLM, it is difficult to draw more conclusive interpretations about the exact origin of the indirect visual input from the present results. Nevertheless, our results show that the indirect input contributes to the output of the LGN neuron and is more significant for larger stimuli. To resolve the exact nature of the indirect visual influence, intracellular recordings with membrane potential of LGN neuron clamped at a high depolarizing value will be required, to reveal the IPSCs more distinctly than was possible in previous studies (Wang et al., 2007).

5 Conclusions

The indirect visual inputs to LGN relay neurons have a modest influence on the visual response. Their contribution is larger for large stimuli, with a polarity opposite to that of the receptive field of the LGN neuron itself. The properties of the indirect inputs are compatible with several possibilities: feedforward inhibition from thalamic interneurons innervated by the same RGC that provides the main drive to the relay cell (locked inhibition), feedforward inhibition from interneurons driven by RGCs other than the main driver (nonlocked inhibition), or feedback projections from the thalamic reticular nucleus. Further experiments with prolonged extracellular recording with spatiotemporal noise stimuli or natural images, or intracellular recording from LGN neurons, or a combination of electrophysiological and anatomical techniques, will be needed to determine the exact source and the spatial extent of these inputs.

6 Acknowledgments

The authors gratefully acknowledge the following grant support. AC: K25 MH67225. EK: NEI EY016371, EY16224, NIGM71558 and Core Grant EY12867. LP: Sloan research fellowship & NSF CAREER award.

References

- Andolina, I. M., Jones, H. E., Wang, W., and Sillito, A. M. (2007). Corticothalamic feedback enhances stimulus response precision in the visual system. *Proc Natl Acad Sci U S A*, 104(5):1685–1690.
- Bishop, P. O. (1953). Synaptic transmission; an analysis of the electrical activity of the lateral geniculate nucleus in the cat after optic nerve stimulation. *Proc R Soc Lond B Biol Sci*, 141(904):362–392.
- Blitz, D. M. and Regehr, W. G. (2005). Timing and specificity of feed-forward inhibition within the lgn. *Neuron*, 45(6):917–928.
- Briggs, F. and Usrey, W. M. (2007). A fast, reciprocal pathway between the lateral geniculate nucleus and visual cortex in the macaque monkey. *J Neurosci*, 27(20):5431–5436.
- Carandini, M., Demb, J. B., Mante, V., Tolhurst, D. J., Dan, Y., Olshausen, B. A., Gallant, J. L., and Rust, N. C. (2005). Do we know what the early visual system does? *J Neurosci*, 25(46):10577–10597.
- Carandini, M., Horton, J. C., and Sincich, L. C. (2007). Thalamic filtering of retinal spike trains by postsynaptic summation. *J Vis*, 7(14):20.1–20.11.
- Casti, A., Hayot, F., Xiao, Y., and Kaplan, E. (2008). A simple model of retina-lgn transmission. *J Comput Neurosci*, 24(2):235–252.
- Cleland, B. G., Dubin, M. W., and Levick, W. R. (1971). Simultaneous recording of input and output of lateral geniculate neurones. *Nat. New Biol.*, 231:191–192.
- Cudeiro, J. and Sillito, A. M. (1996). Spatial frequency tuning of orientation-discontinuity-sensitive corticofugal feedback to the cat lateral geniculate nucleus. *J Physiol*, 490 (Pt 2):481–492.
- Dubin, M. W. and Cleland, B. G. (1977). Organization of visual inputs to interneurons of lateral geniculate nucleus of the cat. *J Neurophysiol*, 40(2):410–427.
- Fiset, P., Paus, T., Daloze, T., Plourde, G., Meuret, P., Bonhomme, V., Hajj-Ali, N., Backman, S. B., and Evans, A. C. (1999). Brain mechanisms of propofol-induced loss of consciousness in humans: a positron emission tomographic study. *J Neurosci*, 19(13):5506–5513.
- Funke, K. and Eysel, U. T. (1998). Inverse correlation of firing patterns of single topographically matched perigeniculate neurons and cat dorsal lateral geniculate relay cells. *Vis Neurosci*, 15(4):711–729.
- Hamos, J. E., van Horn, S. C., Raczkowski, D., and Sherman, S. M. (1987). Synaptic circuits involving an individual retinogeniculate axon in the cat. *J. Comp. Neurol.*, 259:165–192.
- Hochstein, S. and Shapley, R. M. (1976). Quantitative analysis of retinal ganglion cell classifications. *J Physiol*, 262(2):237–264.
- Hubel, D. H. and Wiesel, T. N. (1961). Integrative action in the cat's lateral geniculate body. *J Physiol*, 155:385–398.
- Humphrey, A. L. and Weller, R. E. (1988). Structural correlates of functionally distinct x-cells in the lateral geniculate nucleus of the cat. *J Comp Neurol*, 268(3):448–468.
- Kaplan, E., Purpura, K., and Shapley, R. M. (1987). Contrast affects the transmission of visual information through the mammalian lateral geniculate nucleus. *J Physiol*, 391:267–288.
- Kaplan, E. and Shapley, R. (1984). The origin of the s (slow) potential in the mammalian lateral geniculate nucleus. *Exp Brain Res*, 55(1):111–116.
- Mante, V., Bonin, V., and Carandini, M. (2008). Functional mechanisms shaping lateral geniculate responses to artificial and natural stimuli. *Neuron*, 58(4):625–638.
- Mayo, J. P. (2009). Intrathalamic mechanisms of visual attention. *J Neurophysiol*, 101(3):1123–1125.

- McAlonan, K., Cavanaugh, J., and Wurtz, R. H. (2008). Guarding the gateway to cortex with attention in visual thalamus. *Nature*, 456(7220):391–394.
- Okatan, M., Wilson, M., and Brown, E. (2005). Analyzing functional connectivity using a network likelihood model of ensemble neural spiking activity. *Neural Computation*, 17:1927–1961.
- Paninski, L. (2004). Maximum likelihood estimation of cascade point-process neural encoding models. *Network*, 15(4):243–262.
- Paninski, L., Pillow, J., and Lewi, J. (2007). Statistical models for neural encoding, decoding, and optimal stimulus design. *Prog Brain Res*, 165:493–507.
- Pillow, J. W., Paninski, L., Uzzell, V. J., Simoncelli, E. P., and Chichilnisky, E. J. (2005). Prediction and decoding of retinal ganglion cell responses with a probabilistic spiking model. *J Neurosci*, 25(47):11003–11013.
- Pillow, J. W., Shlens, J., Paninski, L., Sher, A., Litke, A. M., Chichilnisky, E. J., and Simoncelli, E. P. (2008). Spatio-temporal correlations and visual signalling in a complete neuronal population. *Nature*, 454(7207):995–999.
- Rees, G. (2009). Visual attention: the thalamus at the centre? *Curr Biol*, 19(5):R213–R214.
- Reid, R., Victor, J., and Shapley, R. (1997). The use of m-sequences in the analysis of visual neurons: linear receptive field properties. *Vis Neurosci*, 14(6):1015–27.
- Reinagel, P. and Reid, R. C. (2000). Temporal coding of visual information in the thalamus. *J Neurosci*, 20(14):5392–5400.
- Sherman, S. M. (2005). Thalamic relays and cortical functioning. *Prog Brain Res*, 149:107–126.
- Sherman, S. M. and Friedlander, M. J. (1988). Identification of x versus y properties for interneurons in the a-laminae of the cat's lateral geniculate nucleus. *Exp Brain Res*, 73(2):384–392.
- Sherman, S. M. and Guillery, R. W. (1998). On the actions that one nerve cell can have on another: distinguishing "drivers" from "modulators". *Proc Natl Acad Sci U S A*, 95(12):7121–7126.
- Sherman, S. M. and Guillery, R. W. (2002). The role of the thalamus in the flow of information to the cortex. *Philos Trans R Soc Lond B Biol Sci*, 357(1428):1695–1708.
- Shutter, E. E. (1987). *A practical nonstochastic approach to nonlinear time-domain analysis*. In V. Z. Marmarelis (Ed.), *Advanced Methods of Physiological Systems Modeling (vol. 1)*. University of Southern California, Los Angeles.
- Sincich, L. C., Adams, D. L., Economides, J. R., and Horton, J. C. (2007). Transmission of spike trains at the retinogeniculate synapse. *J Neurosci*, 27(10):2683–2692.
- Sincich, L. C., Horton, J. C., and Sharpee, T. O. (2009). Preserving information in neural transmission. *J Neurosci*, 29(19):6207–6216.
- Snyder, D. and Miller, M. (1991). *Random Point Processes in Time and Space*. Springer-Verlag.
- Truccolo, W., Eden, U. T., Fellows, M. R., Donoghue, J. P., and Brown, E. N. (2005). A point process framework for relating neural spiking activity to spiking history, neural ensemble, and extrinsic covariate effects. *J Neurophysiol*, 93(2):1074–1089.
- Uglesich, R., Casti, A., Hayot, F., and Kaplan, E. (2009). Stimulus size dependence of information transfer from retina to thalamus. *Front Syst Neurosci*, 3:10.
- Uhlrich, D. J., Cucchiaro, J. B., Humphrey, A. L., and Sherman, S. M. (1991). Morphology and axonal projection patterns of individual neurons in the cat perigeniculate nucleus. *J Neurophysiol*, 65(6):1528–1541.
- Usrey, W. M., Reppas, J. B., and Reid, C. (1999). Specificity and strength of retinogeniculate connections. *J Neurophysiol*, 82(6):3527–40.

- van Hateren, J. H. (1997). Processing of natural time series of intensities by the visual system of the blowfly. *Vision Res*, 37(23):3407–3416.
- Wang, S., Bickford, M. E., Horn, S. C. V., Erisir, A., Godwin, D. W., and Sherman, S. M. (2001). Synaptic targets of thalamic reticular nucleus terminals in the visual thalamus of the cat. *J Comp Neurol*, 440(4):321–341.
- Wang, X., Wei, Y., Vaingankar, V., Wang, Q., Koepsell, K., Sommer, F. T., and Hirsch, J. A. (2007). Feedforward excitation and inhibition evoke dual modes of firing in the cat’s visual thalamus during naturalistic viewing. *Neuron*, 55(3):465–478.
- Weyand, T. G. (2007). Retinogeniculate transmission in wakefulness. *J Neurophysiol*, 98(2):769–785.